APPLIED AND ENVIRONMENTAL MICROBIOLOGY, Apr. 1985, p. 799–810
0099-2240/85/040799-12$02.00/0

Vol. 49, No. 4

Detection, Enumeration, and Sizing of Planktonic Bacteria by Image-Analyzed Epifluorescence Microscopy

MICHAEL E. SIERACKI, PAUL W. JOHNSON, AND JOHN McN. SIEBURTH*

Graduate School of Oceanography, University of Rhode Island Bay Campus, Narragansett, Rhode Island 02882

Received 30 August 1984/Accepted 11 January 1985

Epifluorescence microscopy is now being widely used to characterize planktonic procaryote populations. The tedium and subjectivity of visual enumeration and sizing have been largely alleviated by our use of an image analysis system consisting of a modified Artek 810 image analyzer and an Olympus BHT-F epifluorescence microscope. This system digitizes the video image of autofluorescing or fluorochrome-stained cells in a microscope field. The digitized image can then be stored, edited, and analyzed for total count or individual cell size and shape parameters. Results can be printed as raw data, statistical summaries, or histograms. By using a stain concentration of 5 μg of 4′6-diamidino-2-phenylindole per ml of sample and the optimal sensitivity level and mode, counts by image analysis of natural bacterial populations from a variety of habitats were found to be statistically equal to standard visual counts. Although the time required to prepare slides, focus, and change fields is the same for visual and image analysis methods, the time and effort required for counting is eliminated since image analysis is instantaneous. The system has been satisfactorily tested at sea. Histograms of cell silhouette areas indicate that rapid and accurate estimates of bacterial biovolume and biomass will be possible with this system.

The complex role of the picoplankton (0.2- to 2.0-μm) and nanoplankton (2.0- to 20.0-μm) size fractions (30) of the aquatic microbial community is currently the focus of considerable study (3, 10, 14, 29, 34, 36). Direct microscopic observations are essential for studying the microbial plankton, and a variety of techniques with epifluorescence microscopy are now available. Direct counting of samples stained by acridine orange (AO) (15, 39), 4′6-diamidino-2-phenylindole (DAPI) (25), or other dyes has become routine for determining picoplankton populations in aquatic environments. Observations by epifluorescence microscopy of small, autofluorescent cells contributed to the discovery of the widespread distribution of chroococcoid cyanobacteria in the open ocean (17, 35) and is now routinely used for their enumeration (3, 20, 21). Other recent applications of epifluorescence microscopy include the determination of the frequency of dividing cells as an indicator of instantaneous growth rate (14, 22), the use of fluorescent antibodies to detect specific bacterial types (4, 7, 26, 34), and the enumeration and differentiation of chloroplast-containing and apochlorotic nanoplankton populations (5, 8, 13, 27). Biomass estimates of bacterial populations often are made visually by measuring epifluorescent images with an ocular micrometer to determine biovolume and then calculating cell carbon by using appropriate conversion factors (6, 9, 10, 12, 22, 36, 38). These visual counting and measuring methods are time consuming and tedious, particularly at sea where microscopy is difficult under the best of conditions.

All of the above visual methods of enumeration and sizing depend upon the analysis of images produced by epifluorescence microscopy and should lend themselves to image analysis with the appropriate equipment. Image analysis of microscopic particles was developed in the 1950s and 1960s for counting coal particles in air (33) and leukocytes in blood (16). The first application of image analysis to epifluorescence microscopy that we are aware of (24) was to count AO-stained bacteria and somatic cells in milk. The data showed that population estimates by Coulter Counter (Coulter Electronics, Inc.), standard plate method, visual microscopy, and the image analyzer correlated well. Our tests with this image analyzer system revealed that the system was not able to detect the bacterial minicells (36) that dominate oceanic samples.

A comparison of different combinations of epifluorescence microscopes, video cameras, and image analyzers within our financial constraints led us to the configuration described here, a state-of-the-art image-analyzed epifluorescence microscope system (hereafter referred to as the system). We now report our results on the application of the system to the detection, counting, and sizing of picoplankton from a variety of both marine and freshwater environments. This semiautomated system has proven to be rapid and accurate for both counting and sizing natural bacterial populations, and its potential for biomass estimation is highly promising.

MATERIALS AND METHODS

Sampling. Samples from Narragansett Bay, Narrow River (an eutrophic, tidal river), and Barber Pond, (a 12-ha, relatively unpolluted freshwater pond), all in Rhode Island, were collected in bottles prerinsed with filtered (pore size, 0.2 μm) distilled water. Samples from the Sargasso Sea were taken by a water sampler aboard the manned Sea-Link submersible of the Harbor Branch Foundation (Station no. 1) or by Niskin bottle from the R/V Endeavor (Station no. 105). Samples from Chesapeake Bay used to test the system aboard ship were also taken by Niskin bottle from the R/V Cape Henlopen. All samples were fixed with 50% biological-grade glutaraldehyde or Formalin (final preservative concentration, 1% vol/vol) and stored at 5°C.

Staining. Several experiments were performed to determine the optimum procedures for detecting, counting, and sizing natural picoplankton populations with the image analyzer. Three stains, DAPI (5.0 μg/ml) (25), Hoescht 33258 (5.0 μg/ml) (23), and AO (0.01%, wt/vol) (15), were compared by using Narragansett Bay picoplankton samples. The

* Corresponding author.

samples were prepared by slight modifications of the epifluorescence direct-count method (15, 25). Samples were first filtered through a 1.0-μm Nuclepore filter to remove large particles, and appropriate volumes were placed in sterile, disposable plastic test tubes and stained for at least 5 min. A carefully prewetted 0.45-μm Gelman filter (GN-6) was first placed on the sintered glass base, to promote an even dispersion of cells, followed by a wet Irgalan black-stained 0.2-μm Nuclepore filter. The stained sample was drawn through the filters (vacuum, <12 cm of Hg), and the Nuclepore filter was immediately placed on a microscope slide which had been fogged by breath to promote adherence. A small drop of silicone (refractive index, 1.404) or standard (Cargille Type A; refractive index, 1.515) immersion oil, depending on which objective lens was used, was quickly placed on top of the filter. A cover glass was added, the edges were sealed with paraffin, and the slides were stored in the dark at 5°C until counted and sized, usually within 48 h. To determine the optimal concentration of DAPI, detection of the same sample stained with DAPI concentrations ranging from 1.1 to 5.0 μg/ml was also tested.

Microscopes. Our first attempts to detect natural populations of DAPI-stained bacteria with the image analyzer were made with an Olympus Vanox microscope equipped for epifluorescence with a 200-W Hg lamp and a standard vidicon tube in the video camera. Bacteria could not be detected with this equipment. With a more sensitive video tube (chalnicon) and a microscope with a brighter fluorescing image (Olympus BHT-F), we obtained a very satisfactory image and detection of all bacteria including the minicells of oceanic samples (28, 36). The Olympus BHT-F microscope, equipped with a 100-W Hg lamp and a 100× silicone oil immersion objective (SI FL100/1.25F), was used with its internal diaphragm wide open. This Olympus objective was used rather than the newer UV FL100/1.35, since the former has less field curvature. Objectives that are corrected for flatness of field (i.e., Olympus S Plan 100/1.25 and S Plan Apo 100/1.35-.80) were also examined but cannot be used since their glass lenses transmit very little of the UV light necessary for DAPI excitation.

Counts were made of several slides from a single sample of Narragansett Bay seawater (NBW) to quantitatively compare the various microscope and objective combinations. Sixteen to thirty fields were counted on each of three to six slides. Grand means of the mean slide counts were compared by the Student *t* test at a 95% level of significance. Two Zeiss microscopes were compared with the Olympus BHT-F: a Standard 14 and a Photoinvertoscope IM35. Both were equipped for epifluorescence with a 50-W Hg lamp and a ×100 oil immersion objective (Neofluar 100/1.30). To compare objective lenses, the Zeiss Neofluar 100 was also used on the BHT-F. The Olympus SI FL100, however, has a shorter barrel and could not be used on either Zeiss microscope. All microscopes had the appropriate UV excitation and barrier filters necessary for the DAPI stain.

Image analyzer. The major components of the Artek 810 image analyzer (Artek Systems Corp., Farmingdale, N.Y.) fitted to an epifluorescence microscope are shown (Fig. 1). It is critical that the Hg lamp be properly focused to assure the brightest possible image. Sensitivity-level potentiometers are located on the model 982 Counter for the two modes of detection available, edge and density. The threshold density level of detection can be set at 1 of 256 grey levels. The front panel of model 982 also has controls for the shape, size, and position of an electronic aperture which defines the area of the field to be analyzed. Model 982 converts the composite video signal into a binary, or digitized, signal, with the image in the format of a grid (512 by 512) of picture elements (pixels). The binary video signal is received by the model 940 Silhouette Memory Unit which stores the digitized image in two memory locations so that editing can be done while retaining an unaltered original image. The stored image is displayed on the image monitor as an enhancement (brightness on the screen) to provide feedback of the digitized image. This enhancement can be in the form of either flags (small bright dots next to each detected object, Fig. 2C) or silhouettes (bright enhancement covering the entire detected area of each object, Fig. 2D). The flags and silhouettes are slightly offset from the object so that both the object and its silhouette can be seen. Editing of the stored, digitized image is performed manually with a light pen on the image monitor to remove extraneous objects or to isolate specific objects for analysis. Measurement data on all or selected objects in the image are accessed through an Apple II+ microcomputer and can be stored on disk for future analysis. The microcomputer also provides control of the model 940 editing and measurement functions and performs the final statistical analyses on the measurement data. The results can then be printed in the form of raw data, statistical summaries, or histograms by a dot matrix printer.

A variety of measurements on each object (cell) in the digitized image can be made, including perimeter, area, longest dimension, longest horizontal chord, horizontal and vertical ferets, circularity (perimeter of a circle with equal area divided by the measured perimeter), and location coordinates. Results can be expressed either in pixels or absolute units (micrometers or micrometers squared), and upper and lower limits can be applied to any parameter, permitting measurement of objects within a specific size range.

Calibration of the image analyzer. To determine a conversion factor from pixels to micrometers for each objective and microscope used, the model 810 system was calibrated with a standard stage micrometer (10 μm per smallest division). By using transmitted light, the image of the stage micrometer was focused on the monitor screen, and a circular electronic aperture was adjusted to three different diameters (30, 40, and 50 μm). For each aperture size the image of the grating was moved out of the field, the aperture was completely filled with enhancement by increasing the sensitivity level, and 10 successive measurements of horizontal chord (diameter) were taken. Machine variation was less than 0.3% of the mean. The mean readings (in pixels) were divided by the known diameter (in micrometers) for each aperture size and then averaged to obtain the scale factor for linear measurement in units of micrometers per pixel. The linear scale factor was squared to yield the area scale factor (micrometers squared per pixel). The software has a one-step, semiautomatic calibration routine, but this was judged not as precise as the above procedure.

Image analysis procedure. Bright field illumination is used to bring the texture of the Nuclepore filter into focus. By using epifluorescence, the cells on the filter surface are then visually focused and scanned at ×1,000 to ensure even distribution. The image is then diverted to the video camera and focused on the image monitor screen. Since detection by the image analyzer is adequate only before significant quenching of the fluorescence occurs (within 10 to 15 s), and the hands are focusing and changing fields, a foot switch is used to quickly freeze the image to memory. Either the silhouette or the flag mode of enhancement can be used while focusing the cells in randomly chosen fields (Fig. 2).

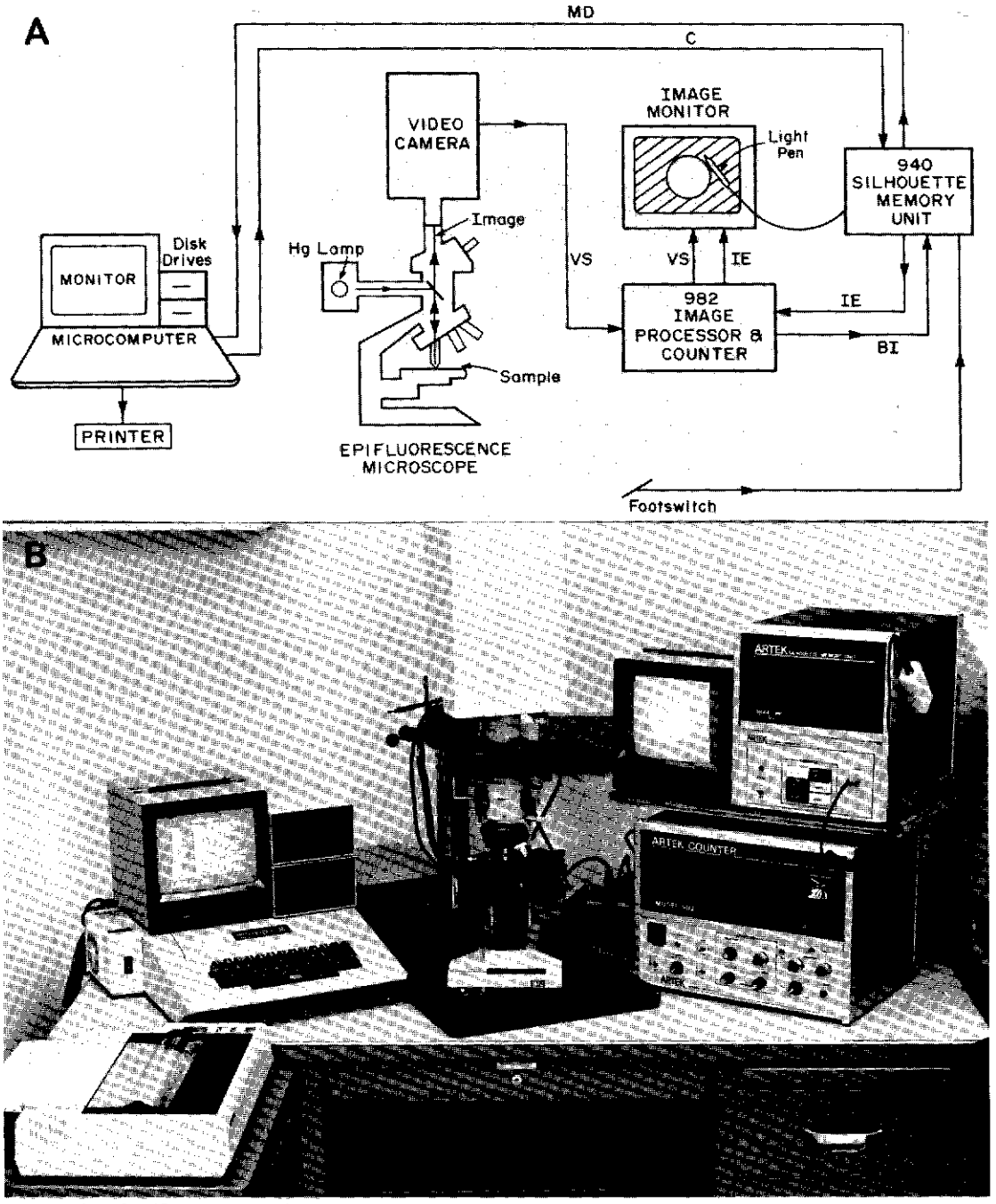

FIG. 1. Image-analyzed epifluorescence microscope system composed of an Olympus BHT-F epifluorescence microscope fitted with the Artek model 810 image analyzer. (A) Schematic diagram. A fluorescent image is formed in the epifluorescence microscope and detected by an enhanced video camera equipped with a sensitive chalnicon tube. The image is sent as a video signal (VS) to the model 982 counter, digitized and displayed on the image monitor, and then sent to the model 940 Silhouette Memory Unit for storage, editing, and analysis. A foot switch causes the binary image (BI) to be stored, and the image can be displayed on the image monitor as enhancements (IE) (see the text and Fig. 2). Editing on the image monitor can be done with the light pen. An Apple II+ microcomputer provides control (C) of the editing functions of the model 940, processes the measurement and count data (MD), stores the data on a disk, and can print it on the printer. (B) Photograph of the system in the laboratory in the same arrangement as that in panel A.

When sizing cells, the complete digitized image is examined on the image monitor by using the silhouette enhancement mode. The sensitivity threshold should be set visually by comparing the object image to the silhouette shape. After freezing the image, the field can be checked by eye through the oculars to compare images. By using the light pen, cells lying across the edge of the aperture or detrital particles can be deleted or specific cells can be isolated for analysis. The light pen allows for interactive, visual discrimination of bacteria from other debris in each field before it is analyzed. The UV shutter should be closed as soon as possible after the image is stored to prevent fading during analysis. Two-

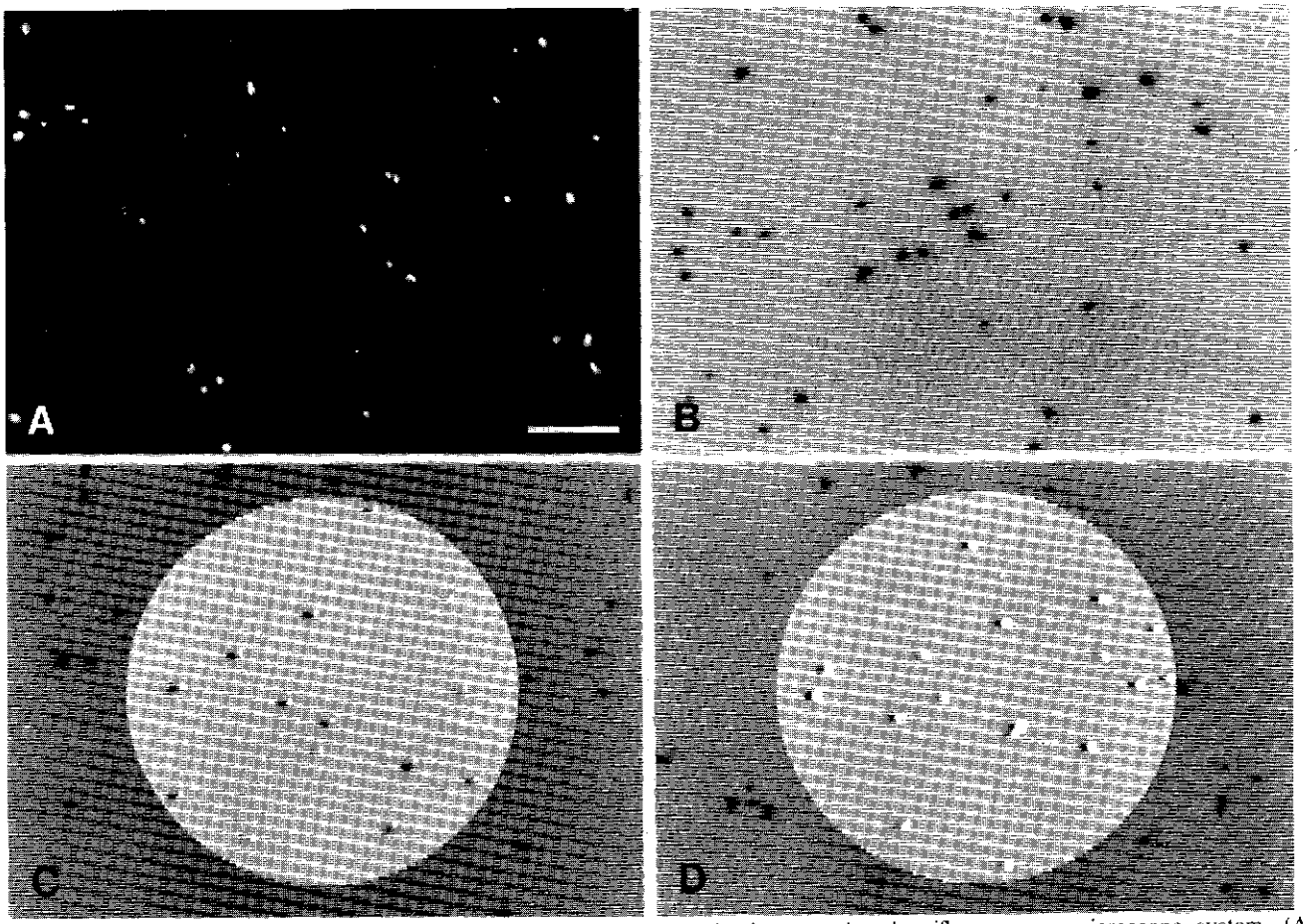

FIG. 2. Images of DAPI-stained Narragansett Bay picoplankton by the image-analyzed epifluorescence microscope system. (A) Photomicrograph of the sample. Close-ups of the image monitor of the system show unenhanced video image (B), image enhanced by flags and circular electronic aperture showing the counted cells (C), and image enhanced by silhouettes showing the cell areas (D). The video image is reversed (B, C, and D) so that the bright fluorescing bacteria (A) appear dark. Bar, 10 μm; all photographs are at the same magnification. The images of both the cells and their enhancements on the monitor appear slightly larger due to the high contrast setting.

key commands from the computer keyboard initiate analysis of the digitized image. When accessing the full menu of parameters and storing the data to disk, analysis takes less than 1 s per object. When analysis is complete, the image is cleared from memory, and the above process is repeated with a new field until an appropriate total number of cells are measured (typically >300). Means, standard deviations, or histograms of any of the measured parameters can be printed at any time. The complete analysis is accomplished with the general analysis software provided by Artek Systems Corp. The model 810 system is a limited programmable system since the software is proprietary but expandable.

The above procedure of randomly selecting a field, focusing, and storing the image with the foot switch is also used when only counting cells. Closing the UV shutter is not required since a one-key count command results in a printed count of the field within 1 s and a new field can immediately be brought into focus. When a predetermined number of fields or cells has been counted, the computer audibly signals the operator, and count statistics can be displayed or printed, including number of fields and cells counted, mean count per field, standard deviation, coefficient of variation, and the conversion to number of cells per milliliter. To do this we modified an interactive program in BASIC, developed by Artek Systems Corp., to accept field counts and perform the appropriate conversion calculations. The sample volume (in milliliters), conversion factor (number of fields per filter), and sample identification are entered before counting begins. Recent software improvements allow rapid, simultaneous counting and sizing of cells in the same fields.

Comparison of visual and image analysis counts. Comparison counts between the image-analyzed and standard eye counts of the same fields were made in the following manner. A circular paper aperture was placed in one of the microscope eyepieces, and the electronic aperture of the image analyzer was adjusted to exactly match the size and position of the ocular aperture. Each randomly chosen field was first counted with the image analyzer and then by eye so that fading during the visual count would not affect the image-analyzed count. Individual field counts by the two methods were compared by a paired Student *t* test (31).

Growth experiment. To observe changes in the size distribution of a natural bacterial population over time, a dilution-growth experiment was conducted. NBW (14°C) was collected off the Narragansett Bay Campus dock during an incoming tide. By using sterile filtration apparatus, this water was sequentially and aseptically filtered through a Gelman (type A/E) glass-fiber filter, a 0.45-μm filter (Millipore Corp.), and finally through a 0.2-μm Nuclepore filter to substantially reduce the bacteria. Vacuum was maintained

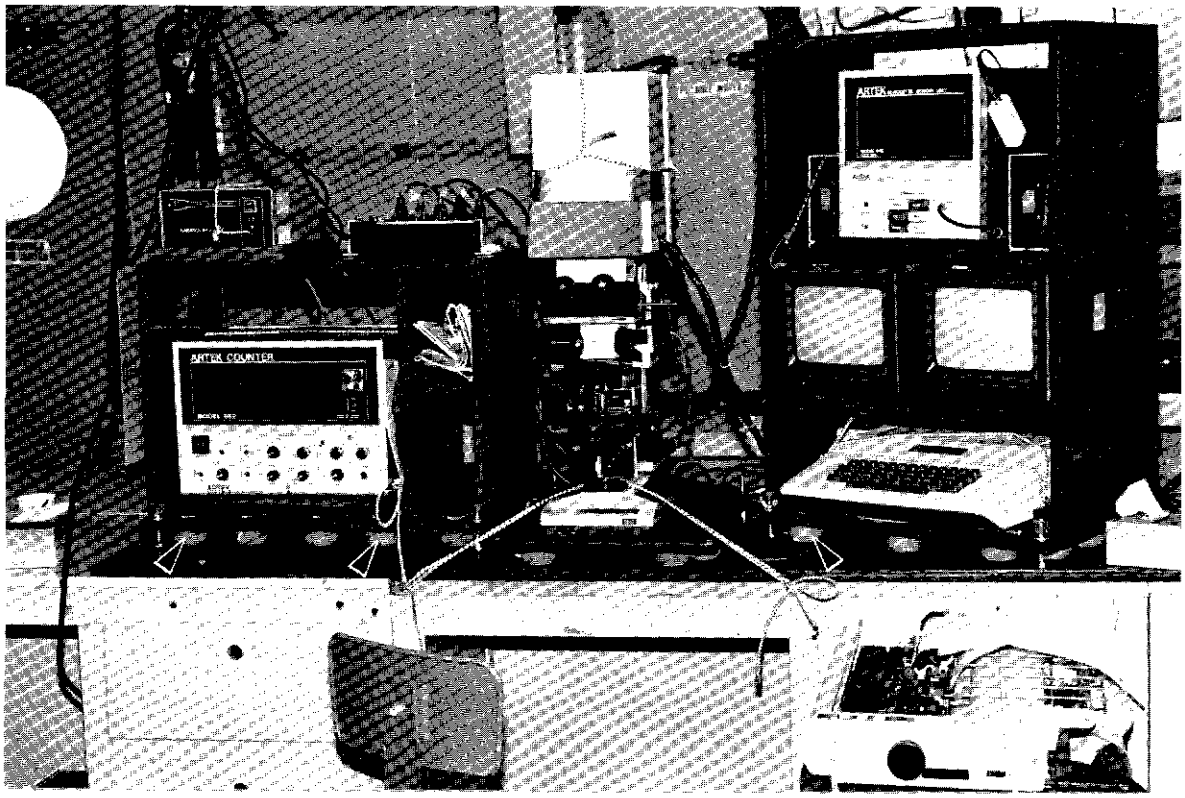

FIG. 3. Image-analyzed epifluorescence microscope system securely packaged for operation at sea to reduce the effects of the vibration of the ship. Note the use of racquet balls (arrows) and shock cords to secure gear.

below 30 cm of Hg at all times. A subsample of the Gelman A/E filtrate was then aseptically passed through a 0.6-μm Nuclepore filter to yield an inoculum containing unattached, free-living bacteria. The remaining preparative steps were conducted by sterile techniques under a laminar flow hood. The inoculum was added to the essentially bacteria-free NBW at a 1:100 dilution. The inoculated NBW was mixed with a magnetic stirrer for 10 min and then dispensed into four 250-ml Teflon FEP bottles (Nalge Co.). Two bottles served as replicate controls with no further additions, whereas the other two bottles were augmented with the following addition of nutrients (per liter): NH_4Cl (25 mg), NaH_2PO_4 (10 mg), and Fe-sequestrene (5 mg). One of these bottles also received glucose at a final concentration of 1 mg/liter. The bottles were incubated in a 20°C water bath and periodically sampled over 46 h. Samples were taken aseptically under the laminar flow hood and fixed, stored, and analyzed as described above.

Use aboard ship. The Prophot IV cruise aboard the R/V Cape Henlopen in Chesapeake Bay (May 1984) and an R/V Endeavor cruise (12 July 1984) afforded opportunities to test the susceptibility of the microscope-image analysis system to the vibrations and electrical fluctuations aboard ship. The system was configured (Fig. 3) with model 982, model 940, monitors, computer, and disk drives mounted in compartmentalized plywood boxes. These component boxes and the microscope were mounted on racquet balls to dampen vibration. Bolts or shock cords held the equipment in place.

RESULTS

Optimization of stains and detection. The system was able to detect bacteria regardless of the stain used. It was observed, however, that DAPI did not quench as rapidly as Hoescht 33258 or AO under the bright excitation illumination of the BHT-F and therefore allowed more time for focusing. More importantly, DAPI is a vital stain for DNA and does not stain detritus as the others do. For these reasons, DAPI is the stain of choice. Detection by the system was optimal at a concentration of 5 μg/ml, and even cells with diameters of <0.2 μm were adequately detected. The slower fading at this stain concentration allowed sufficient time for all cells to be focused and stored in memory for accurate analysis by the system.

The ability of the image analysis epifluorescence microscope system to detect and count DAPI-stained picoplankton in edge and density detection modes and over a range of settings on the sensitivity potentiometers is compared with a visual count (Fig. 4). The edge counts are consistently higher than the density counts since in the density mode the analyzer only detected the large, bright cells. At a sensitivity setting of 9.75 in the density mode, the small bacterial cells were not detected and the count was actually noise (i.e., the aperture was filled with "snow"). The count in the density mode was unsatisfactory for the picoplankton since the visual count yielded a value of 45.4 (± 6.85) cells per field (or 1.52×10^6 [$\pm 0.23 \times 10^6$] cells per ml). In the edge detection mode, however, all cells were adequately detected before significant machine noise appeared. The extremely high count at an edge sensitivity of 8.5 was due to noise. Settings of 7.5 and 8.0 in this mode gave excellent detection, as observed on the monitor, and the resulting counts were not significantly different from the visual count.

Once the optimum procedures and instrument settings were determined, quantitative detection of the smallest

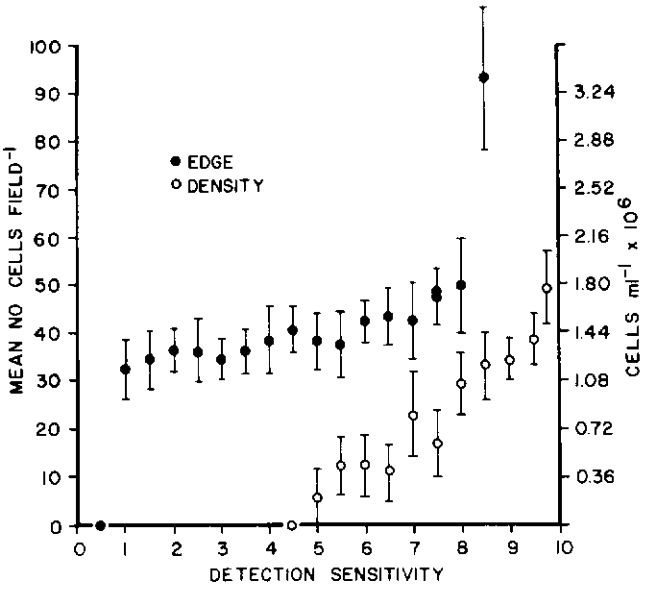

FIG. 4. Ability of the system to detect and count DAPI-stained cells from a Narragansett Bay picoplankton sample in edge and density detection modes over a range of instrument sensitivity settings. The error bars represent 1 standard deviation. The visual count of this sample was 45.4 (±6.85) cells per field (or 1.52×10^6 [$\pm 0.23 \times 10^6$] cells per ml).

bacteria by the system was excellent (Fig. 2). Detection was best with the camera in the reverse video mode due to better contrast. Flag enhancements for both counting and sizing are used to focus the video image of the cells (Fig. 2C). When sizing cells it is necessary to use silhouette enhancements (Fig. 2D) so that the digitized image can be directly compared to the video image.

The detection of autofluorescing cells from cultures of the photosynthetic cyanobacterium *Synechococcus* is excellent. Under blue-light excitation, they fluoresce red or orange, which is near the peak sensitivity of the camera. Because they are significantly larger (diameter, 1 to 2 μm) than most nonphotosynthetic bacteria, the best detection of these chroococcoid cyanobacteria was achieved with the density mode. Initial observations with AO-stained nanoflagellate cultures and a 40× objective have shown that the density detection mode allowed these cells to be detected, whereas the smaller, more numerous bacteria fluorescing in the background were not detected.

TABLE 1. Comparison of three microscopes and two 100× objectives used with the image-analyzed epifluorescence microscope system, showing the quantitatively better detection by the Olympus BHT-F/Zeiss objective combination

Microscope	Objective[a]	n[b]	Mean count[c] of cells per field	SD
Olympus BHT-F	O	3	17.73	0.42
Zeiss IM-35	Z	4	18.62	0.76
Zeiss Standard 14	Z	6	14.38[d]	1.13
Olympus BHT-F	Z	5	20.68[e]	0.80

[a] O, Olympus SI FL 100/1.25F; Z, Zeiss Neofluar 100/1.30.
[b] n, Number of slides counted.
[c] A total number of 16 to 30 fields were counted per slide.
[d] Significantly lower at the 95% level of significance.
[e] Significantly higher at the 95% level of significance.

Calibration of the system. For the Olympus BHT-F microscope, the scale factors determined for linear measurement were 0.20 μm per pixel (Olympus 100× objective) and 0.19 μm per pixel (Zeiss 100× objective). The area scale factors are, therefore, 0.040 and 0.036 μm^2 per pixel, respectively. When the Zeiss microscopes and the Zeiss 100× objective were used, the scale factors for linear measurement were determined to be 0.25 μm per pixel (IM-35) and 0.28 μm per pixel (Standard 14) with area scale factors of 0.063 and 0.078 μm^2 per pixel, respectively.

Comparison of microscopes and objectives. Results of the comparison counts with three microscopes and two objectives are shown in Table 1. The grand means of the mean slide counts were compared. In the comparison between the Zeiss IM-35 and the BHT-F, each with its own objective, the grand means of the counts per field were not statistically different. When the Zeiss objective was used on the BHT-F, however, the mean count was significantly higher. This difference between objectives on the BHT-F was also apparent in the eyepieces, as the Zeiss objective produced a much brighter image compared with the Olympus objective and therefore detected more of the smallest fluorescing objects. In the comparison between the Zeiss Standard 14 microscope and the BHT-F (with both Olympus and Zeiss objectives), the grand mean of the counts by the Olympus microscope with either objective was significantly higher than that by the Standard 14. Measurements of individual

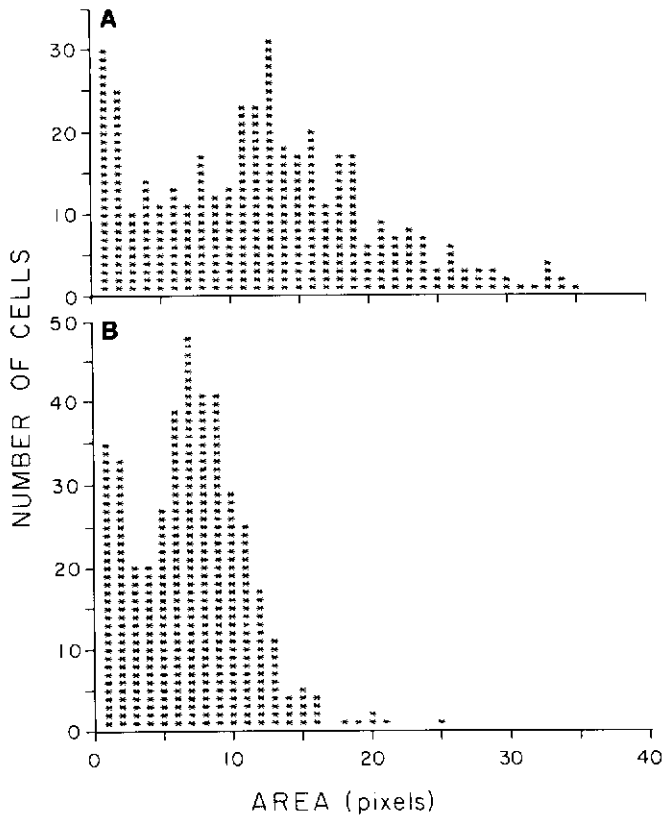

FIG. 5. Comparison of the area histograms of DAPI-stained cells from Narragansett Bay analyzed with the Zeiss Neofluar 100/1.30 objective with the Olympus BHT-F microscope (A) and the Zeiss Standard 14 microscope (B). The same slide was used for both measurements. These histograms are as generated by the computer but with the axes drawn in.

cell areas (in pixels) were made while counting, and the resulting area histograms (Fig. 5) show a wider distribution of cell sizes with the BHT-F versus a more compact grouping with the Standard 14. This difference is due to the lower magnification, and the consequently higher scale factor, of the Zeiss Standard 14-Artek 810 combination. These histograms are software generated and show the quality produced directly by the dot matrix printer.

Comparison of visual and image analysis counts. Comparisons between visual- and image-analyzed counts are summarized in Table 2. The concentrations of total bacteria extended over nearly two orders of magnitude from 1.5×10^5/ml in the deepest Sargasso Sea sample to 1.2×10^7/ml in the eutrophic Narrow River. None of the mean counts were significantly different at the 95% significance level by the paired t test.

Size distributions of picoplankton populations. The ability of the system to size the picoplankton from various environments is illustrated (Fig. 6). These histograms are also of the image silhouette areas in units of pixels and were made by using the Olympus microscope and the Olympus objective (1 pixel = 0.04 μm^2). The Barber Pond sample (Fig. 6C) is characterized by a large number of very small (<6-pixel) blue-fluorescing particles. The proportion of objects in this size range is notably smaller in the Sargasso Sea and Narragansett Bay samples (Fig. 6A and B). Only a small proportion of the Barber Pond bacteria are larger than 10 pixels in area, whereas the means of both the Narragansett Bay and Sargasso Sea bacteria are larger than 10 pixels. The shapes of the area distribution of the Narragansett Bay and Sargasso Sea samples are quite smaller, although the Sargasso Sea sample has a somewhat sharper peak in the 7- to 13-pixel range and fewer cells of <5 pixels.

Growth experiment. The dilution and incubation of natural Narragansett Bay bacteria yielded a standard logistic growth curve over 46 h (Fig. 7A). The curves for the control condition (Fig. 7) are the mean of the two replicate bottles, whereas the enriched condition represents the single bottle which contained both glucose and the inorganic nutrients. The bottle containing only inorganic nutrients was similar in response to the two control conditions and is not shown in Fig. 7. The addition of nutrients resulted in an earlier onset

TABLE 2. Comparison of bacterial counts from a variety of habitats of the same fields by the image-analyzed epifluorescence microscope system and by eye

Sample station	Depth (m)	No. of fields	Mean count per field		Bacterial cells (10^6)/ml	Paired t test[b]
			Eye	Artek		
Sargasso Sea						
1	30	15	24.73	25.40	0.35	−1.03
1	130	14	21.00	21.57	0.30	−0.81
105	50	15	38.80	37.93	0.54	1.27
105	100	15	23.27	22.60	0.33	1.00
105	200	15	13.79	13.29	0.15	0.78
Narragansett Bay						
I		15	34.53	32.20	2.20	1.75
II		15	36.80	37.13	2.24	−1.19
III		15	33.87	31.53	2.16	1.72
Narrow River		15	56.40	59.73	11.51	−1.16
Barber Pond		15	42.33	40.93	4.13	1.25

[a] Mean of eye and Artek counts.
[b] None were significant at the 95% confidence level.

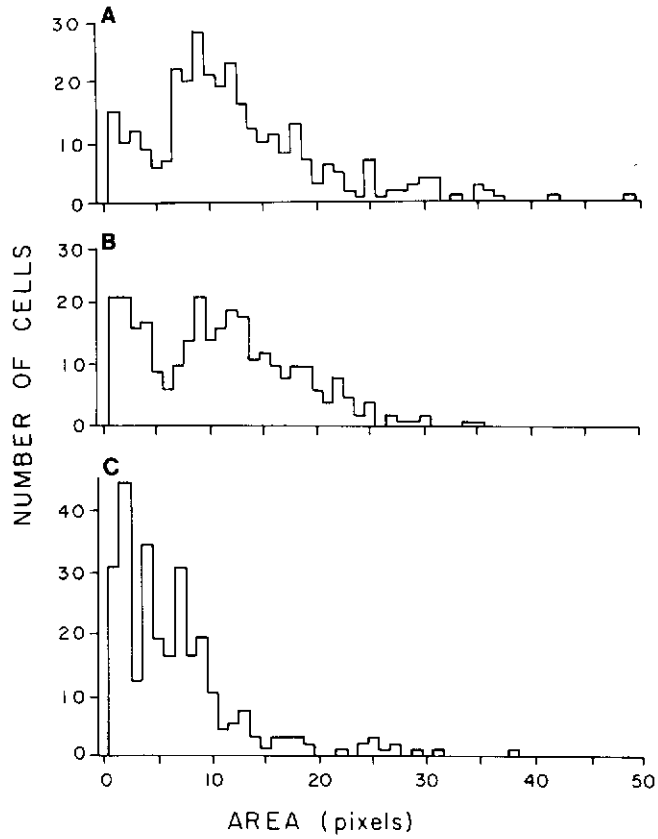

FIG. 6. Histograms (redrawn from computer printout) of the silhouette areas of natural populations of DAPI-stained picoplankton populations from Sargasso Sea (A), Narragansett Bay (B), and Barber Pond (C). 1 pixel = 0.04 μm^2.

of exponential growth and a more rapid growth rate than those in the unenriched seawater (Fig. 7A). Enrichment also resulted in cells with a greater mean area (Fig. 7B). The increase in mean cell area in the enriched seawater was visually apparent through the microscope. Large rods were present singly and in clumps of two to eight cells in the last five samples. The clumps were much less numerous than single cells and were edited out of the image before size analysis so that the mean area values (Fig. 7B) and the resulting histograms (Fig. 8) represent only single cells. A slight increase in the mean area of cells occurred in the controls between 17 and 29 h. This was a much smaller change relative to that in the enriched condition and is probably due to an increase in the number of dividing cells. The size distributions of the control and enriched conditions remained quite similar through the first 17 h (Fig. 8A). During the period of most rapid growth (24 to 32 h), however, the large rods, with areas greater than ca. 30 pixels, became apparent only in the enriched condition (Fig. 8B and C). By 40 h the unimodal area distributions of the two conditions were quite similar (Fig. 8D), although the mean area of the enriched population was slightly higher (Fig. 7B).

Biovolume estimations. Bacterial biovolume estimates calculated from the measured mean silhouette areas of the three samples of natural populations and some of the growth experiment samples (Fig. 7) are shown in Table 3. Estimates are shown under two assumptions: (i) spherical cells (the maximum potential volume) and (ii) prolate spheroid cells

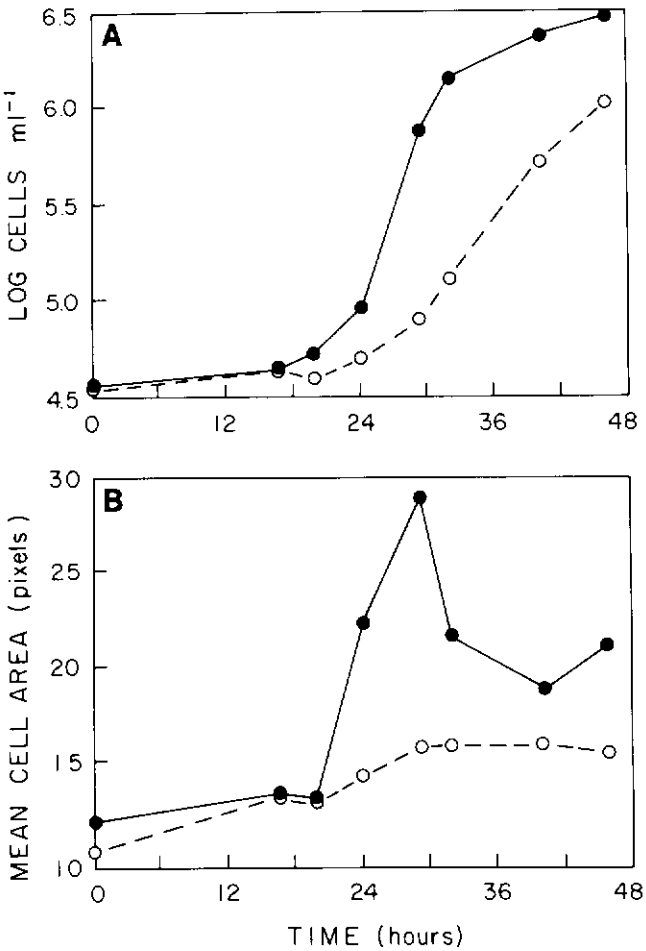

FIG. 7. Use of the system to follow changes in cell number (A) and mean cell area (B) during the growth of natural populations of Narragansett Bay bacteria with (●) and without (○) the addition of glucose and inorganic nutrients.

with a length-to-width ratio of 2. These are approximations based only on the area measurements. The 2.2× increase in cell area in the enriched flask between 17 and 29 h corresponds to a 3.2× increase in biovolume (assuming spheres).

Use aboard ship. On the R/V Cape Henlopen, the racquet ball mounting system required some slight adjustments (replacement of bolts on the microscope stand with shock cords) to minimize the marked vibration of the ship, especially at higher speeds. Moderate electrical disturbance was encounted sporadically when the compressor of the ship was turned on, causing a change in electrical frequency. This put the video camera and the model 982 image processor out of synchronization and temporarily destroyed the image. When the air conditioner was turned on later during the cruise, making the frequency and synchronization problems persistent, image analysis was impossible.

The identical setup was also tested on board the R/V Endeavor. During this sea trial, however, an uninterruptible 750-W power supply (Sola Electric, Elk Grove Village, Ill.) was used as well as the 20-kW "clean" power supply permanently installed in the laboratory area of the ship. The system performed almost perfectly, with only some slight noise encountered near the maximum threshold settings of sensitivity.

DISCUSSION

This study, the first to apply image analysis technology to epifluorescent images of aquatic bacterial populations, demonstrates the ability of the system to accurately detect, enumerate, and size planktonic bacteria. Our data comparing visual with image-analyzed counts (Table 2) revealed no significant difference. The higher specificity of DAPI and the high contrast provided by our system have allowed accurate and precise enumeration of even the smallest aquatic bacteria.

The initial application of image analysis to epifluorescence microscopy was for semiautomated counting of bacteria and somatic cells in milk (24). These authors were well aware of the advantage that the automation of epifluorescence counting would have in alleviating operator fatigue. The results of this study showed good correlation between visual and image-analyzed epifluorescence counts and also plate and Coulter counts. The resolution of this system was only 0.345 μm per pixel, however, and our trials with this same system indicated that it was not able to detect the smaller bacteria and larger viruses in seawater samples and therefore was not adequate. By contrast, the system described here has a resolution of 0.19 μm per pixel, almost double the resolving power.

Choosing the proper microscope and lens combination is essential for adequate fluorescence, image intensity, and magnification. Optimal detection, counting, and sizing requires: (i) a higher stain concentration than that for counts by eye, (ii) proper focusing of the 100-W Hg lamp and, (iii) the use of a foot switch to freeze the image to memory. An operator familiar with microscopy can learn in a very short time to change fields, fine focus, press the foot switch, and access the count, all within several seconds.

Speed of counting and sizing. The time to randomly select, focus, and count a field with the system was found to average 6 s and was independent of the number of cells in the field. This compares with the estimate for visual counting by Kirchman et al. (18) of 30 s per field over a wide range of field counts (<10 to >70 cells per field) and with our estimate of 40 s for field counts near 50 cells per field. This means that image analysis reduces the time required to count a sample by 85%.

An optimal sampling scheme for the system was determined by the cost-variance optimizing formulas from Sokal and Rohlf (32) and the results from the analysis of variance on the Ice House Pond sample reported by Kirchman et al. (18). For the purpose of comparison we also used the Kirchman et al. (18) estimates of cost (time) for subsampling (2 min) and filter preparation (5 min). The resulting optimum scheme for counting by the system is to take three subsamples, prepare one filter from each, and count 15 fields on each filter. The total time when this scheme is used is 21 min per sample, and the expected total variance on this sample would be 3.3. This is a 13% reduction in time and a 38% reduction in variation relative to the Kirchman et al. (18) estimates based on the optimal scheme for counting by eye (time, 24 min; variation, 5.3). Counting two subsamples would save more time but would be at the cost of less precision. Additional significant time reduction is achieved by the computer tabulation of field counts and calculations of count means, variation, and resulting cell concentration. With the image analysis system the investigator instantly receives this data upon completing each slide.

The time required to analyze a sample depends upon whether only count data or also size information is desired.

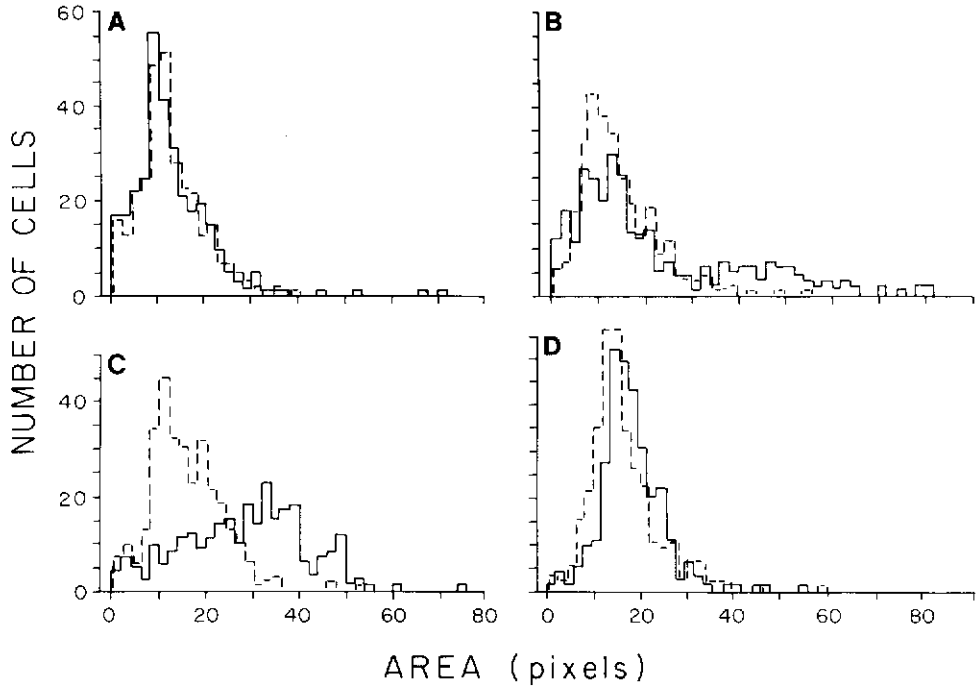

FIG. 8. Area histograms of bacteria from the growth experiment in Fig. 7, showing changes in the size distributions over time. The enriched (——) and control (-----) populations remained similar through 17 h (A), but the added nutrients selected for a larger cell type by 24 h (B) which rapidly became dominant (29 h, C). Upon apparent nutrient depletion at 40 h (D) the size distributions were again similar. 1 pixel = 0.036 μm^2.

The system acquires cell number and cell parameters of a whole field within milliseconds. The output of count data alone is rapid. The procedure for simultaneous counting and sizing takes longer than counting alone since data must be taken for each cell in the field and stored on disk. Each cell is measured and stored in less than 1 s. During the testing of the system at sea aboard the R/V Cape Henlopen, it was found that the average slide takes from 15 to 20 min to analyze for both count and area, depending on the density of cells on the filter and the amount of editing (if any) required. Software improvements and a 16-bit computer are expected to decrease this time significantly.

Size distributions of bacterial populations. Our sizing data demonstrate that much valuable information about picoplankton populations can be obtained when simultaneous size measurements are taken with the count data. The general shapes of the area histograms of natural populations (Fig. 6) show a surprising similarity between Narragansett Bay and Sargasso Sea populations. Upon closer examination, however, it can be seen that the Narragansett Bay sample had more cells in the 1- to 4-pixel size range than did the Sargasso Sea sample, whereas the main peak of the Sargasso population was more pronounced and at a slightly smaller size than the corresponding peak of the Narragansett Bay sample. This suggests that the Sargasso Sea population is less diverse in size than that of Narragansett Bay. The Barber Pond histogram is distinctly different from the other two, with a pronounced abundance of small, 1- to 5-pixel-sized objects. This sample was examined in thin sections by transmission electron microscopy, and it was found that a "bloom" of both bacterial (100-nm) and algal (300-nm) viruses was present (unpublished data). The system was probably detecting the larger algal viruses in this sample as objects in the 1- to 2-pixel size range.

The growth experiment further illustrates the advantage of size measurements in conjunction with cell numbers for characterizing bacterial populations and processes. The growth response of natural bacterial populations in the control (Fig. 7A) is typical of numerous similar experiments conducted in our laboratory (2; M. E. Sieracki and J. McN. Sieburth, unpublished data) and by others (1). The addition of nutrients caused a shortened lag period and more rapid growth relative to those of the control, but the population curves generally paralleled each other. The cell area data, however, show that the nutrient enrichment caused a pronounced increase in mean cell size and, ultimately, a population of larger cells (Fig. 7B). The increase in mean area between 20 and 29 h in the enriched condition reflects the increase in the number of large rods undergoing rapid division. The different responses of the bacteria to the two conditions are seen in the area histograms (Fig. 8). Although the shape of the histograms in the control did not change appreciably over time, the addition of nutrients caused a distinct extension of the distribution curve towards large cell areas during the period of most rapid population growth (Fig. 8B). The large rods are dominant in the 29-h sample (Fig. 8C), but the distribution soon returned to a shape similar to that of the control (Fig. 7D), presumably due to nutrient depletion. The resulting biomass changes due to enrichment are greater than those indicated by changes in cell numbers alone. The simultaneous estimation of bacterial numbers and size will be very useful in studying the trophodynamics of bacterial growth and their predation by bacterivorous protozoa (8, 29). One of the reasons for developing this system is to observe the diel changes in numbers and size due to nutrition, photo-induced dormancy, and predation (1–3, 29).

Biovolume estimations. The estimates of mean cell biovolume (Table 3) show both the maximum potential values (assuming spheres) and a probably more realistic estimate,

assuming prolate spheroids with a length-to-width ratio of 2. The biovolume estimates of the natural populations compare favorably with published values based on visual measurements by epifluorescence microscopy. Ferguson and Rublee (10) found an average of 0.09 μm^3 per cell in coastal waters. For samples from waters off Woods Hole, Mass., Watson, et al. (36) reported a similar value in one sample and 0.28 μm^3 per cell in another. More recently, Fuhrman and Azam (12) reported bacterial volumes ranging from 0.08 to 0.14 μm^3 per cell in the coastal waters of British Columbia, and Fuhrman (11) reported averages of 0.03 and 0.18 μm^3 per cell in two samples off the southern California coast. In growth experiments of marine bacterioplankton in unenriched seawater culture (1) mean cell biovolumes ranged from 0.10 to 0.25 μm^3. These variations in reported cell biovolumes demonstrate that cell numbers alone cannot be used to accurately estimate the contribution of the picoplankton to the total microbial biomass.

Scanning electron microscopy has also been used to determine bacterial cell biovolume (19). As Fuhrman has shown, however, estimates of cell biovolume by scanning electron microscopy are not accurate due to cell shrinkage of up to 37% (11). Measurements of transmission electron micrographs, though probably more accurate, are even more time consuming than visual epifluorescence microscopy or scanning electron microscopy. The biovolume estimates (Table 3) are only approximate since they were made under the assumption of either uniformly spherical or prolate spheroid cells, although actual cell shapes vary with size. The estimates by other authors noted above are somewhat better, being based on individual cell measurements or, more often, on averages of specified size and shape categories. These measurements are tedious and time consuming when done visually. The information available from the digitized silhouette images of the image analyzer, however, allows such measurements to be made rapidly. Algorithms are presently being developed in conjunction with Artek Systems Corp. to determine biovolumes of individual cells based on perimeter, width, length, longest dimension, circularity, and area. These measurements will be used to classify cells as spheres, prolate spheroids, or cylinders and to calculate biovolume and biomass accordingly.

TABLE 3. Estimates of mean cell biovolumes from the silhouette areas by the image-analyzed epifluorescence microscope system, assuming spherical or prolate spheroid cells

Sample	n	Mean area		Mean cell biovolume (μm^3)	
		Pixels	μm^2[a]	Sphere[b]	Prolate spheroid[c]
Natural populations					
Sargasso Sea (100 m)	319	12.69	0.51	0.27	0.19
Narragansett Bay	301	11.11	0.44	0.22	0.16
Barber Pond	274	6.88	0.28	0.11	0.08
Growth experiment					
Control					
17 h	610	13.15	0.47	0.24	0.17
24 h	600	14.28	0.51	0.27	0.19
29 h	628	15.73	0.57	0.32	0.23
40 h	629	15.86	0.57	0.32	0.23
Enriched					
17 h	313	13.22	0.48	0.25	0.18
24 h	308	22.28	0.80	0.54	0.38
29 h	269	28.84	1.04	0.80	0.56
40 h	301	18.89	0.68	0.42	0.30

[a] The scale factor for natural populations (Olympus objective) was 1 pixel = 0.040 μm^2 and for growth experiment (Zeiss objective) was 1 pixel = 0.036 μm^2.

[b] The spherical biovolume = $4/3\ \sqrt{A^3/\pi}$, where A = silhouette area in micrometers squared.

[c] The prolate spheroid biovolume = $0.94\ \sqrt{A^3/\pi}$ (length-to-width ratio = 2).

Image analysis at sea. The current trend towards automated analytical procedures at sea is now yielding close to real time data and is allowing the detailed study of such short-term phenomenon as blooms, anoxia, and diel events which were previously recognized only months or years after they occurred when preserved samples were analyzed. During several days of operation of the system at sea, the counting and sizing of cells became quite routine. The total time required to focus, edit nonbacterial particles, count and size images, and print the count statistics and area histograms with the prototype software took 20 min per slide. Recent software improvements by Artek Systems Corp. and our laboratory should halve this time. The ability to rapidly and accurately count and size the bacteria makes it possible for a two-person team to do a sufficient number of vertical profiles to be able to observe diel changes in in situ populations.

Limitations of image analysis. It must be emphasized that the accuracy of this system depends entirely upon the quality of the primary image. The configuration chosen was made on this basis. Clear, bright images with few unwanted particles (fluorescing detritus, etc.) are required for good detection and rapid enumeration. The problem of detrital material is largely overcome by the high specificity of DAPI for living cells. We have observed that large bacterial cells in culture or from rich environments yield an uneven fluorescence with DAPI, presumably due to the heterogeneous distribution of DNA in the cell. AO or other whole-cell stain may be required for accurately sizing such populations. A similar situation exists with the nanoplankton since DAPI stains only the nuclear material. Detrital fluorescence may be a problem with less specific stains, especially in coastal and estuarine waters. Another problem encountered mainly in culture work is the clumping of cells. Although individual cells in small aggregates can often be differentiated visually, this task is difficult if not impossible with the system working only with two-dimensional silhouettes. A recently developed procedure for disaggregating bacteria in clumps and from particles with pyrophosphate, followed by sonification, may be useful in this regard (M. I. Velji, M.S. thesis, Simon Fraser University, Burnaby, British Columbia, Canada, 1983).

Some shrinkage of the silhouettes can be noticed within the first second or two of illumination, but they subsequently stabilize well before the image is focused and stored. Our size measurements generally agree with previously made measurements, albeit a wide range has been reported. The precision of the biovolume estimation presently being developed would be limited primarily by the resolution of the system. The resolution with the 100× objective (0.036 μm^2/pixel) means that most bacterial cell silhouettes are defined by 7 to 20 pixels (Fig. 5A and 6). This is probably enough information to yield estimates of biovolume at least as accurate as those obtained visually. The shape of cells with areas below 5 or 6 pixels cannot, of course, be determined as precisely as larger cells so that the biovolume estimate will be less accurate for these smaller cells. The same is true, however, for visual size estimates.

Potential applications. The determination of frequency of dividing cells for natural populations of chroococcoid cyanobacteria may be possible by using area measurements, in combination with other parameters such as longest dimension, perimeter, and circularity, and discriminant analysis techniques. Based on our observations, however, it is doubtful that frequency of dividing or divided cells could be accurately determined for the smaller nonphotosynthetic picoplankton by image analysis. Larger bacterial cells in culture, however, may provide enough information for single and dividing cells to be distinguished, as demonstrated by the large dividing cells that appeared in our growth experiment (Fig. 6B).

Initial observations indicate that the detection and enumeration of the eucaryotic cells in the nanoplankton by this system should be satisfactory. This will be useful in studies of nanoflagellate predation rates upon bacteria, an area of current interest (29).

We are currently developing the application of this system to fluorescent antibody techniques to determine the distribution and abundance of specific trophic types of bacteria. Particularly, we are developing fluorescent antibody methods to detect the methane-oxidizing (J. McN. Sieburth, P. W. Johnson, M. Eberhardt, and M. E. Sieracki. 1984. EOS **64**:1054) and methylamine-oxidizing bacteria (J. McN. Sieburth and P. W. Johnson, unpublished data) that have been recently obtained from pelagic waters. This system would also be a useful complement to flow cytofluorometry now being developed for plankton research (37). Since these powerful instruments are not quantitative, they require postsorting quantification by epifluorescence microscopy.

We have found that the Artek 810 image analyzer–Olympus BHT-F system is an excellent tool for rapidly enumerating and sizing autofluorescent and fluorochrome-stained picoplankton populations. The potential for biovolume and biomass estimation has been demonstrated, and the development and calibration of these measurements are the thrust of our current work.

ACKNOWLEDGMENTS

We thank Michael Reeve, formerly of the Biological Oceanography Program of the National Science Foundation, who had the vision to provide supplementary funds for this system and Dick Chiasson, Mike Huns, Jonathan Strater, and Bill Kitchener for invaluable help in the selection of the microscopic and image analysis equipment. The development and testing of this application have been with the welcome cooperation of Mike Bender and his associates at Artek Systems Corp. We acknowledge Marsh Youngbluth of the Harbor Branch Foundation for arranging for the Sea-Link samples, Dean Stockwell for collecting the R/V Endeavor 105 Sargasso Sea samples, and Elijah Swift for use of the Zeiss Standard 14 microscope. Nancy Sibilla is thanked for help with manuscript preparation. J.McN.S. thanks Mary A. Tyler for the opportunity to participate on the PROPHOT IV cruise aboard the R/V Cape Henlopen supported by National Science Foundation grant OCE 83-10407.

This work was supported by the Biological Oceanography Program of the National Science Foundation through grant OCE 81-21881.

LITERATURE CITED

1. **Ammerman, J. W., J. Fuhrman, A. Hagström, and F. Azam.** 1984. Bacterioplankton growth in seawater. I. Growth kinetics and cellular characteristics in seawater cultures. Mar. Ecol. Prog. Ser. **18**:31–39.
2. **Baxter, M., and J. McN. Sieburth.** 1984. Metabolic and ultrastructural response to glucose of two eurytrophic bacteria isolated from seawater at different enriching concentrations. Appl. Environ. Microbiol. **47**:31–38.
3. **Burney, C. M., P. G. Davis, K. M. Johnson, and J. McN. Sieburth.** 1982. Diel relationships of microbial trophic groups and in situ dissolved carbohydrate dynamics in the Caribbean Sea. Mar. Biol. **67**:311–322.
4. **Campbell, L., E. J. Carpenter, and V. J. Iacono.** 1983. Identification and enumeration of marine chroococcoid cyanobacteria by immunofluorescence. Appl. Environ. Microbiol. **46**:553–559.
5. **Caron, D. A.** 1983. Technique for enumeration of heterotrophic and phototrophic nanoplankton, using epifluoresence microscopy, and comparison with other procedures. Appl. Environ. Microbiol. **46**:491–498.
6. **Christian, R. R., R. B. Hanson, and S. Y. Newell.** 1982. Comparison of methods for measurement of bacterial growth rates in mixed batch cultures. Appl. Environ. Microbiol. **43**: 1160–1165.
7. **Dahle, A. B., and M. Laake.** 1982. Diversity dynamics of marine bacteria studied by immunofluorescent staining on membrane filters. Appl. Environ. Microbiol. **43**:169–176.
8. **Davis, P. G., and J. McN. Sieburth.** 1982. Differentiation of phototrophic and heterotrophic nanoplankton populations by epifluorescence microscopy. Ann. Inst. Oceanogr. **58**(Suppl.): 249–260.
9. **Ferguson, R. L., E. N. Buckley, and A. V. Palumbo.** 1984. Response of marine bacterioplankton to differential filtration and confinement. Appl. Environ. Microbiol. **47**:49–55.
10. **Ferguson, R. L., and P. Rublee.** 1976. Contribution of bacteria to standing crop of coastal plankton. Limnol. Oceanogr. **21**: 141–145.
11. **Fuhrman, J. A.** 1981. Influence of method on the apparent size distribution of bacterioplankton cells: epifluorescence microscopy compared to scanning electron microscopy. Mar. Ecol. Prog. Ser. **5**:103–106.
12. **Fuhrman, J. A., and F. Azam.** 1982. Thymidine incorporation as a measure of heterotrophic bacterioplankton production in marine surface waters: evaluation and field results. Mar. Biol. **66**:109–120.
13. **Haas, L. W.** 1982. Improved epifluorescence microscopy for observing planktonic micro-organisms. Ann. Inst. Oceanogr. **58**(Suppl.):261–266.
14. **Hagström, A., U. Larsson, P. Hörstedt, and S. Normack.** 1979. Frequency of dividing cells, a new approach to the determination of bacterial growth rates in aquatic environments. Appl. Environ. Microbiol. **37**:805–812.
15. **Hobbie, J. E., R. J. Daley, and S. Jasper.** 1977. Use of Nuclepore filters for counting bacteria by fluorescence microscopy. Appl. Environ. Microbiol. **33**:1225–1228.
16. **Ingram, M., and K. Preston, Jr.** 1970. Automatic image analysis of blood cells. Sci. Am. **223**:72–82.
17. **Johnson, P. W., and J. McN. Sieburth.** 1979. Chroococcoid cyanobacteria in the sea: a ubiquitous and diverse phototrophic biomass. Limnol. Oceanogr. **24**:928–935.
18. **Kirchman, D., J. Sigda, R. Kapuscinski, and R. Mitchell.** 1982. Statistical analysis of the direct count method for enumerating bacteria. Appl. Environ. Microbiol. **44**:376–382.
19. **Krambeck, C., H.-J. Krambeck, and J. Overbeck.** 1981. Microcomputer-assisted biomass determination of plankton bacteria on scanning electron micrographs. Appl. Environ. Microbiol. **42**:142–149.
20. **Krempkin, D. W., and C. W. Sullivan.** 1981. The seasonal abundance, vertical distribution, and relative microbial biomass of chroococcoid cyanobacteria at a station in southern California coastal waters. Can. J. Microbiol. **27**:1341–1344.
21. **Li, W. K. W., D. V. Subba Rao, W. G. Harrison, J. C. Smith, J. J. Cullen, B. Irwin, and T. Platt.** 1983. Autotrophic picoplankton in the tropical ocean. Science **219**:292–295.
22. **Newell, S. Y., and R. R. Christian.** 1981. Frequency of dividing cells as an estimator of bacterial productivity. Appl. Environ. Microbiol. **42**:23–31.
23. **Paul, J. H.** 1982. Use of Hoechst dyes 33258 and 33342 for enumeration of attached and planktonic bacteria. Appl. Environ. Microbiol. **43**:939–944.
24. **Pettipher, G. L., and U. M. Rodrigues.** 1982. Semi-automated

counting of bacteria and somatic cells in milk using epifluorescence microscopy and television image analysis. J. Appl. Bacteriol. **53**:323–329.
25. **Porter, K. G., and Y. S. Feig.** 1980. The use of DAPI for identifying and counting aquatic microflora. Limnol. Oceanogr. **25**:943–948.
26. **Reed, W. M., and P. R. Dugan.** 1979. Study of developmental stages of *Methylosinus trichosporium* with the aid of fluorescent-antibody staining techniques. Appl. Environ. Microbiol. **38**:1179–1183.
27. **Sherr, B., and E. Sherr.** 1983. Enumeration of heterotrophic microprotozoa by epifluorescence microscopy. Est. Coast. Shelf Sci. **16**:1–7.
28. **Sieburth, J. McN.** 1979. Sea microbes. Oxford University Press, New York.
29. **Sieburth, J. McN., and P. G. Davis.** 1982. The role of heterotrophic nanoplankton in the grazing and nurturing of plankton bacteria in the Sargasso and Caribbean Seas. Ann. Inst. Oceanogr. **58**(Suppl.):285–296.
30. **Sieburth, J. McN., V. Smetacek, and J. Lenz.** 1978. Pelagic ecosystem structure: heterotrophic compartments of the plankton and their relationship to plankton size fractions. Limnol. Oceanogr. **23**:1256–1263.
31. **Snedecor, G. W., and W. G. Cochran.** 1978. Statistical methods, 6th ed., p. 94. Iowa State University Press, Ames.
32. **Sokal, R. R., and F. J. Rohlf.** 1969. Biometry. W.H. Freeman & Co., San Francisco.
33. **Walton, W. H.** 1952. Automatic counting of microscopic particles. Nature (London) **169**:518–520.
34. **Ward, B. B., and M. J. Perry.** 1980. Immunofluorescent assay for the marine ammonium-oxidizing bacterium *Nitrosococcus oceanus*. Appl. Environ. Microbiol. **39**:913–918.
35. **Waterbury, J. B., S. W. Watson, R. R. Guillard, and L. E. Brand.** 1979. Widespread occurance of a unicellular, marine, planktonic cyanobacterium. Nature (London) **77**:293–294.
36. **Watson, S. W., T. J. Novitsky, H. L. Quinby, and F. W. Valois.** 1977. Determination of bacterial number and biomass in the marine environment. Appl. Environ. Microbiol. **33**:940–946.
37. **Yentsch, C. M., K. Paul, K. Horan, K. Muirhead, Q. Dortch, E. Haugen, L. LeGrandre, L. S. Murphy, M. J. Perry, D. A. Phinney, S. A. Pompani, R. W. Spinrad, M. Wood, C. S. Yentsch, and B. J. Zahurancc.** 1983. Flow cytometry and cell sorting: a technique for analysis and sorting of aquatic particles. Limnol. Oceanogr. **28**:1275–1280.
38. **Zimmermann, R.** 1977. Estimation of bacterial number and biomass by epifluorescence microscopy and scanning electron microscopy, p. 103–120. *In* G. Rheinheimer (ed.), Microbial ecology of a brackish water environment. Springer-Verlag KG, Berlin.
39. **Zimmermann, R., and L. A. Meyer-Reil.** 1974. A new method for fluorescent staining of bacterial populations on membrane filters. Kiel. Meeresforsch. **30**:24–27.